

Kinetic Analysis of Non-isothermal decomposition of $(\text{Mg}_5(\text{CO}_3)_4(\text{OH})_2 \cdot 4\text{H}_2\text{O} / 5\text{Cr}_2\text{O}_3)$ Crystalline Mixture

Asma. A. Al-Othman*, Khalid. A. Al-Farhan and Refaat. M. Mahfouz

Department of Chemistry, College of Science, King Saud University,
Riyadh, Saudi Arabia

Corresponding author. Email: asmaalothman@yahoo.com

(Received 25/01/1429.; accepted for publication 13/04/1429H.)

Keywords: Thermal decomposition, model fitting, model free, isokinetic, kinetic parameter, MgCr_2O_4 spinel.

Abstract. Pure MgCr_2O_4 spinel was synthesized from crystalline mixture of $(\text{Mg}_5(\text{CO}_3)_4(\text{OH})_2 \cdot 4\text{H}_2\text{O} / 5\text{Cr}_2\text{O}_3)$ by heating at 900°C for 27 h. TG, DTA, FT-IR and XRPD techniques were used to follow the reactions and identify the products. Nonisothermal kinetics of thermal decomposition of un-irradiated and γ -irradiated physical crystalline mixtures were studied in static air. The kinetic parameters were obtained through model-fitting and model-free methods, and artificial isokinetic relationship (IKR) for multi-step processes. The results show that the decomposition for both un-irradiated and γ -irradiated mixtures proceed through two steps with different reaction mechanisms. The first is a third-order reaction (F_3) mechanism followed by one-dimensional diffusion (D_1) as a second step.

Introduction

The tremendous increase in the development of the industrial and transportation sectors have led to consumption of huge quantities of fuel which results in an increase in the amount of hazardous gases such as NO_x , CH_4 and CO_x emitted to the environment. Low cost transition metal mixed oxides such as spinels are active in catalytic total oxidation processes aimed at limiting of air pollution, which often is carried out on the more expensive noble metal-based catalysts. Spinels with AB_2O_4 formula such as pirochromite MgCr_2O_4 have additional important technological applications such as magnetic materials, high temperature ceramics, combustion catalysis, catalytic support, strength agents, sensor elements and inter connection materials for solid oxide fuel cells (Shimizu, *et al.* 1990, Gengembre, *et al.* 1999 and Docherty, *et al.* 2001). MgCr_2O_4 is normal spinel has space group $F3dm$, with 56 atoms per unit cell ($Z=8$), Mg and Cr ions occupy the tetrahedral and octahedral site respectively (Bhatta, *et al.* 2002).

Thermal decomposition of various compounds are of major importance because of their frequent applications in calcinations metallurgy and in the production of large-surface materials for sorbents and

catalysis (Hartman, *et al.* 1994). Many studies have been carried out on the effect of γ -irradiation on the thermal decomposition of inorganic solids (Monshi, *et al.* 1998 and Mahfouz, *et al.* 59, 2000). In general, the effects with increasing dose are in changing of the induction period and acceleration of the decomposition process i.e. the decrease in time or temperature required to complete the reaction in case of the pre-irradiated material which were attributed to formation of additional nucleation site and reactive center (Mahfouz, *et al.* 363, 2000).

In the present work, we report the kinetic studies of the thermal decomposition of crystalline mixtures $(\text{Mg}_5(\text{CO}_3)_4(\text{OH})_2 \cdot 4\text{H}_2\text{O} / 5\text{Cr}_2\text{O}_3)$ before and after γ -irradiation by applying model fitting and model free kinetic approaches to the nonisothermal thermoanalytical data. Formation of magnesium chromite from above materials is also reported. TG, DTA, FT-IR and XRPD techniques were used to follow the reactions and identify the products.

Experimental

Powder of heavy magnesium carbonate hydrate $\text{Mg}_5(\text{CO}_3)_4(\text{OH})_2 \cdot 4\text{H}_2\text{O}$ and Cr_2O_3 were obtained commercially from (BDH reagent grade) and were used without any further purifications. 1:5 molar ratio

mixtures of the starting materials were calcined at different temperature in the range (100-900 °C) for 9 h each. For irradiation, samples were encapsulated under vacuum in glass vials and were exposed to successively increasing doses of γ -irradiation at constant intensity using Co-60 γ -ray cell 220 (Nordion MDS, Intario, Canada) at a dose rate of 10² kGy/h. The source was calibrated against Fricke ferrous sulfate dosimeter, and the dose rate in the irradiated samples was calculated by applying appropriate corrections on the basis of photon mass attenuation and energy-absorption coefficient for the sample and the dosimeter solution (Spinks, *et al.* 1990). IR spectra were recorded as KBr pellets using a Perkin-Elmer 1000 FT-IR spectrometer. XRPD measurements were carried out on a Jeol D8030 X-ray diffractometer using a nickel filter (CuK α λ =1.5418 Å). The thermal decomposition of physical mixture was followed by nonisothermal (dynamic) thermogravimetric techniques using TGA-7 (Perkin-Elmer) thermogravimetric analyzer. Dyanamic experiments were performed at heating rate 5, 10, 15, 20 and 25 °C/min.

Result and Discussion

X-ray powder diffraction (XRPD) analysis

Figure 1 shows XRPD patterns of the calcined mixtures at different temperatures for different duration times. All phases in the mixtures were identified by FARHAN program (Al-Farhan, 1999). The XRPD pattern of the mixture heated at 300 °C displays only the peaks of Cr₂O₃, indicating that the heavy magnesium carbonate hydrate had converted to amorphous lower carbonate as documented by FT-IR measurement (see Fig. 2). The XRPD of the mixture calcined at 500 °C shows only the characteristic peaks of Cr₂O₃ and MgO. No notable changes in XRPD of the mixtures heated up to 600 °C were detected compared with that heated at 500 °C. The XRPD of the mixture calcined at 625 °C are dominated by the peaks of Cr₂O₃ and MgO, with the main characteristic peaks of MgCr₂O₄ just starting to show up in the XRPD. MgCr₂O₄ becomes the dominant phase in the mixture calcined at 900 °C for 9h. MgCr₂O₄ is the only phase present in the XRPD pattern of the mixture heated at 900 °C for 27h. The same result was obtained from the counterpart of irradiated mixture.

FT-IR analysis

Figure 2 shows the FT-IR spectra of the starting materials before and after γ -irradiation. The spectrum of un-irradiated heavy magnesium carbonate hydrate (a) shows bands of the carbonate anion at 1120 cm⁻¹ (symmetric stretching), 1485 and 1423 cm⁻¹ (asymmetric stretching), 745 and 714 cm⁻¹ (symmetric bend), and 854, 886 and 797 cm⁻¹ (asymmetric bend). The two main bands at 3515 and 3450 cm⁻¹ are due to lattice water vibration and the 3649 cm⁻¹ is due to OH⁻ stretching (White, *et al.* 1971). Spectrum (c) shows five main bands at 637, 569, 443, 415 and 305 cm⁻¹ which are due to lattice vibration of un-irradiated Cr₂O₃. Neither disappearance nor appearance of new bands was observed as result of γ -irradiation up to 10³ kGy total γ -ray dose as well as seen in (b and d respectively).

The FT-IR spectra for the calcined mixtures are shown in Fig. 3. The spectra of the mixture calcined at 300 °C shows main bands at 643, 573, 442, 413 and 305 cm⁻¹ which are due to Mg-O and Cr-O lattice vibrations, and the weak band at 858 cm⁻¹ is due to carbonate anion. At 500 °C, the spectra displays, in addition to, lattice vibration bands of MgO and Cr₂O₃, two bands at 957 and 834 cm⁻¹ which are due to Cr=O stretching of amorphous α -MgCrO₄ (Roy, *et al.* 1969). At 625 °C, the bands of α -MgCrO₄ completely disappeared from the spectra, and the characteristic band of MgCr₂O₄ at 429 cm⁻¹ (Williey, *et al.* 1993) is not detectable, although it present and it was confirmed by XRPD. However, the 429 cm⁻¹ band is observable in FT-IR spectra of the mixture heated at 650 °C. The spectra of the mixture calcined at 900 °C for 27h displays only the bands of MgCr₂O₄, and the characteristic band of Cr₂O₃ at 305 cm⁻¹ is completely disappeared.

TG and DTA analysis

Figure 4 shows TG and DTA curves for thermal decomposition of heavy magnesium carbonate in a pure form and in physical mixture with chromium(III)oxide.

Figure 4(a) shows typical TG-DTA curves of the thermal decomposition of pure heavy magnesium carbonate hydrate. The TG of pure salt showed three overlapped decomposition steps. The first decomposition step was in the range of (100 – 250) °C attributed to loss of water of crystallization, this decomposition was accompanied by an endothermic peak at 230 °C. The second decomposition step was

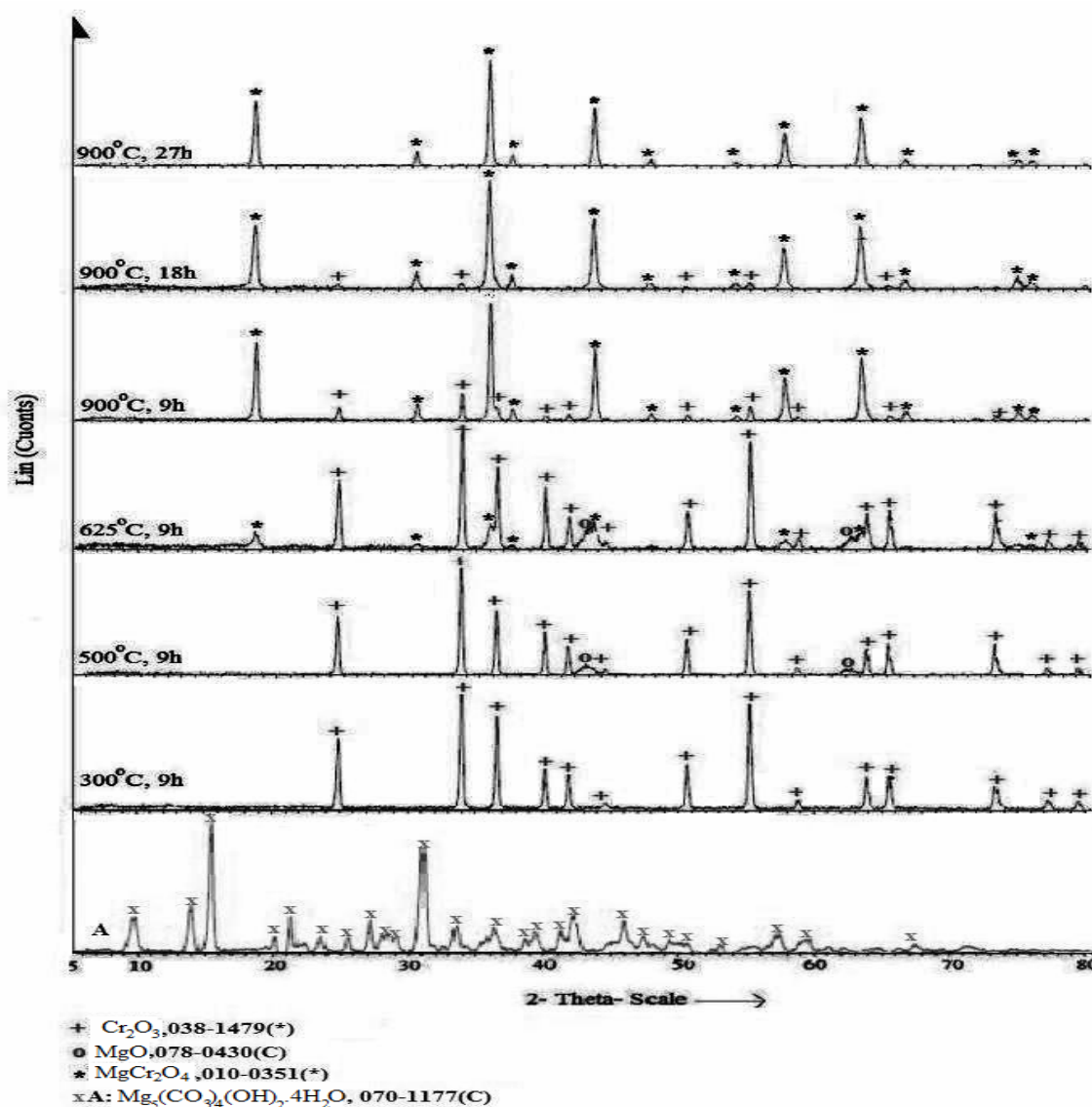


Fig. 1. XRPD patterns of un-irradiated $(Mg_5(CO_3)_4(OH)_2 \cdot 4H_2O)$ and the calcined un-irradiated mixtures at different temperatures for different time duration.

in the range of $(370 - 440)^\circ C$ due to loss of hydroxyl water and was accompanied by an endothermic peak at $430^\circ C$. the third decomposition step was in the range of $(440-500)^\circ C$ due to decomposition of $MgCO_3$ and was accompanied by sharp endothermic peak at $480^\circ C$. Very sharp exothermic peak was detected at $460^\circ C$ attributed to the crystallization of $MgCO_3$ from the amorphous lower carbonate (Khan, *et al.* 2001, Sawada, *et al.*, 32, 1979, Sawada, *et al.* 33, 1979 and Sawada, *et al.*

34, 1979).

Figure (1b) shows the TG and DTA curves of crystalline mixture. The DTA show an endothermic peak detected at almost the same temperature range as for pure salt for loss of water of crystallization. A more broad second endothermic peak was detectable at $440^\circ C$ due to loss of hydroxyl water and starting to form the chromate intermediate. Two endothermic peaks were detectable at $490^\circ C$ and $500^\circ C$ due to the decomposition of chromate intermediate and

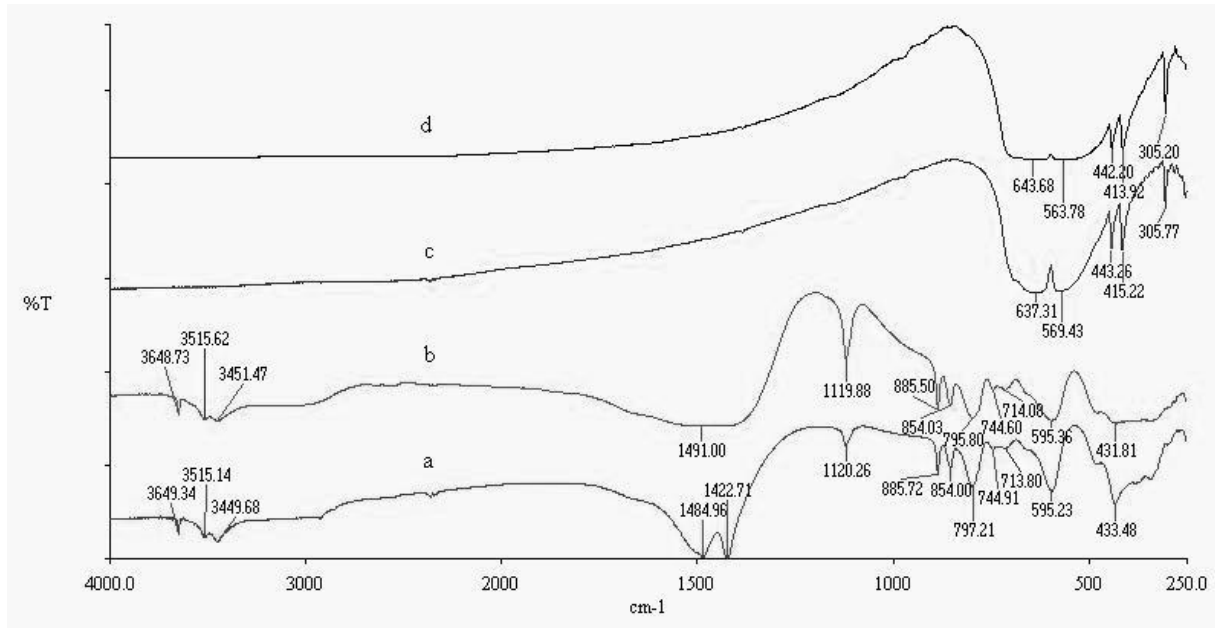


Fig. 2. FT-IR spectra of un-irradiated (a and c) and irradiated (b and d) of Mg₅(CO₃)₂(OH)₂·4H₂O and Cr₂O₃ respectively.

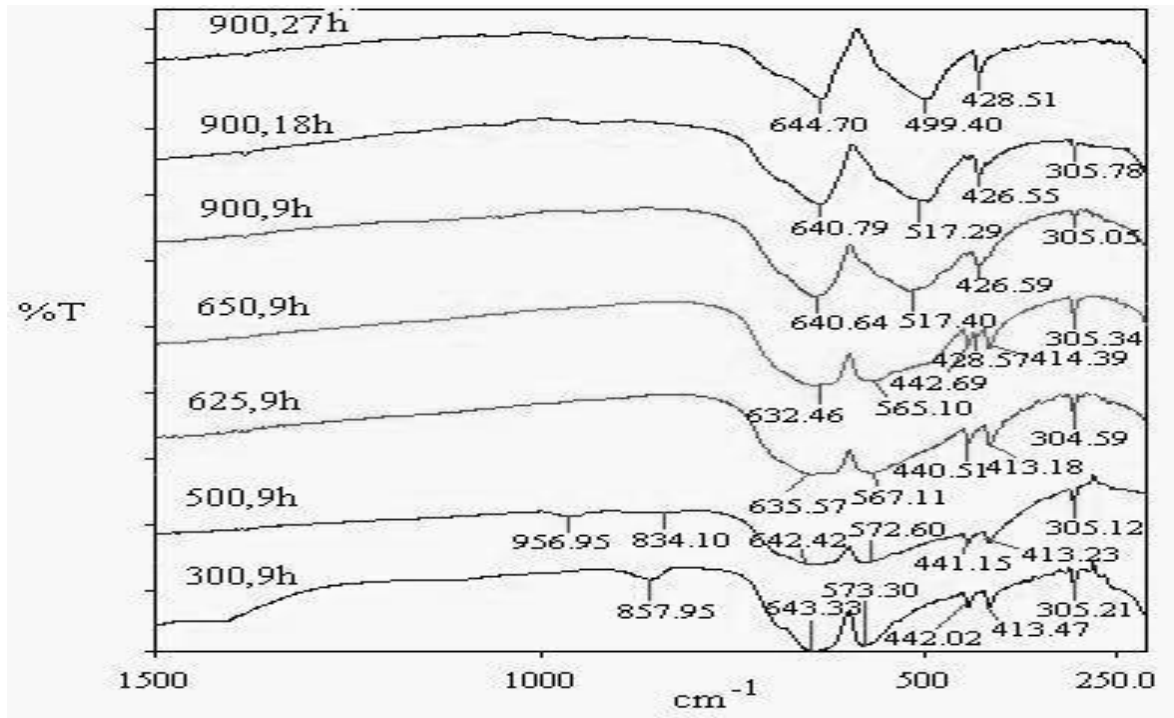


Fig. 3. FT-IR spectra of un-irradiated calcined mixtures at different temperatures for different time duration.

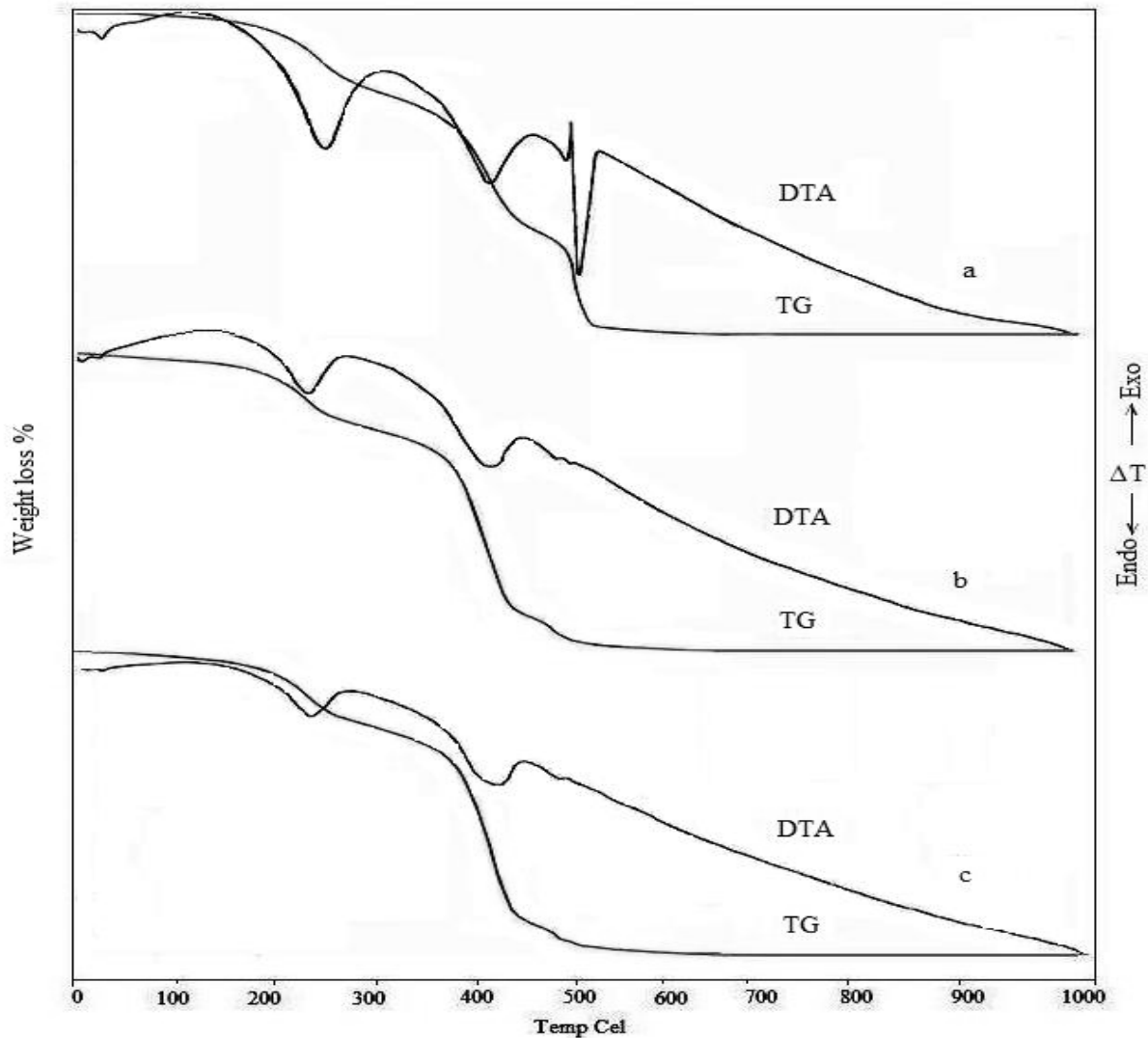


Fig. 4. TG/DTA curves of $Mg_5(CO_3)_4(OH)_2 \cdot 4H_2O$ (a), physical crystalline mixtures before (b) and after (c) irradiation.

formation of amorphous magnesium chromite. The decomposition behavior of γ -irradiated mixture is similar to that of un-irradiated mixture as we seen in fig. (1c). Thus, γ -irradiation has no apparent effect on the decomposition behavior of γ -irradiated physical mixture with 10^2 kGy total dose.

Based on the foregoing discussion of XRPD, FT-IR, TG and DTA analysis the following scheme 1, for decomposition of the investigated crystalline mixture and formation of chromite spinel could be suggested:

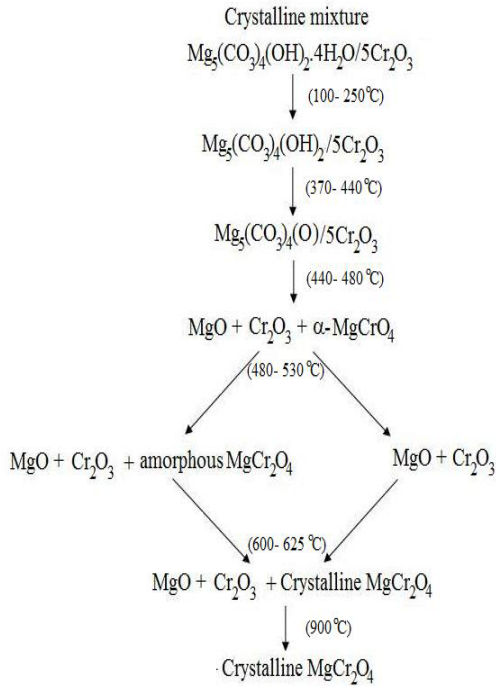
Kinetic studies

Heterogeneous solid-state reaction can empirically

be described by a single-step kinetic equation:

$$\frac{d\alpha}{dt} = k(T)f(\alpha) \quad (1)$$

Where t is the time (min^{-1}), T is the temperature (K), k is the reaction rate constant, α is the extent of conversion ($\alpha = \{W_0 - W / W_0 - W_\infty\}$); W_0 is the initial weight of the sample (mg), W is the sample weight (mg) at any temperature T and W_∞ is the final sample weight (mg), $d\alpha/dt$ is the reaction rate (min^{-1}) and $f(\alpha)$ is the reaction model. The reaction model may



Scheme 1. The proposed reaction mechanism or the thermal decomposition of the investigated crystalline mixture and formation of chromite spinel.

take various forms (Sharp, *et al.* 1966 and Galway, *et al.* 1999), some of which are given in Table 1.

The rate constant, k , usually has an Arrhenius temperature dependence

$$k = A \exp\left(\frac{-E_a}{RT}\right) \quad (2)$$

Where A (min^{-1}) is pre-exponential factor, E_a is the activation energy (kJmol^{-1}) and R is the universal gas constant.

Replacing $k(T)$ in Eq. (1) with the Arrhenius equation gives

$$\frac{d\alpha}{dt} = A \exp\left(\frac{-E_a}{RT}\right) f(\alpha) \quad (3)$$

Under a nonisothermal condition, at constant heating rate $\beta = dT/dt$ Eq. (3) may be written as

$$\frac{d\alpha}{dT} = \frac{d\alpha}{dt} \left(\frac{1}{\beta}\right) = \frac{A}{\beta} \exp\left(\frac{-E_a}{RT}\right) f(\alpha) \quad (4)$$

Upon integration Eq. (4) gives

$$g(\alpha) = \frac{A}{\beta} \int_0^T \exp\left(\frac{-E_a}{RT}\right) dT \quad (5)$$

If E_a/RT is replaced by (x) and integration limits are transformed then Eq. (5) becomes

Table 1. Algebraic expressions of $f(\alpha)$ and $g(\alpha)$ for the reaction models considered in the present work

No.	Symbol	Reaction model	$f(\alpha)$	z
1	D_1	One-dimensional diffusion	$1/2\alpha$	α^2
2	D_2	Two-dimensional diffusion (bi-dimensional particle shape)	$1/[-\ln(1-\alpha)]$	$(1-\alpha)\ln(1-\alpha)+\alpha$
3	D_3	Three-dimensional diffusion (tri-dimensional particle shape) Valensi equation	$3(1-\alpha)^{1/3}/2[(1-\alpha)^{-1/3}-1]$	$[1-(1-\alpha)^{1/3}]^2$
4	D_4	Three-dimensional diffusion (tri-dimensional particle shape) Jander equation	$3/2[(1-\alpha)^{-1/3}-1]$	$(1-2\alpha/3)-(1-\alpha)^{2/3}$
5	R_2	Phase-boundary controlled reaction (contracting area, i.e., bi-dimensional shape)	$2(1-\alpha)^{1/2}$	$[1-(1-\alpha)^{1/2}]^2$
6	R_3	Phase-boundary controlled reaction (contracting volume, i.e., tri-dimensional shape)	$3(1-\alpha)^{2/3}$	$[1-(1-\alpha)^{1/3}]^3$
7	F_1	First-order (Mampel)	$(1-\alpha)$	$[-\ln(1-\alpha)]$
8	F_2	Second-order	$(1-\alpha)^2$	$(1-\alpha)^{-1}-1$
9	F_3	Third-order	$(1-\alpha)^3$	$(1/2)[(1-\alpha)^{-2}-1]$
10	$F_{3/2}$	Three-halves order	$(1-\alpha)^{3/2}$	$2[(1-\alpha)^{-1/2}-1]$
11	A_2	Avrami-Eroféev ($n=2$)	$2(1-\alpha)[- \ln(1-\alpha)]^{1/2}$	$[- \ln(1-\alpha)]^{1/2}$
12	A_3	Avrami-Eroféev ($n=3$)	$3(1-\alpha)[- \ln(1-\alpha)]^{2/3}$	$[- \ln(1-\alpha)]^{1/3}$
13	$A_{3/2}$	Avrami-Eroféev ($n=1.5$)	$(3/2)(1-\alpha)[- \ln(1-\alpha)]^{1/3}$	$[- \ln(1-\alpha)]^{2/3}$
14	A_4	Avrami-Eroféev ($n=4$)	$4(1-\alpha)[- \ln(1-\alpha)]^{3/4}$	$[- \ln(1-\alpha)]^{1/4}$

$$g(\alpha) = \frac{AEa}{\beta R} \int_0^\infty \frac{e^{-x}}{x^2} dx \quad (6)$$

Equation (6) can be written as

$$g(\alpha) = \frac{AEa}{\beta R} P(x) = \frac{A}{\beta} I(Ea, T) \quad (7)$$

The exponential integral (P(x)) has no analytical solution but has many approximations (Khawam, *et al.* 2005).

Kinetic parameters can be obtained from nonisothermal rate laws by both model fitting and isoconversional (model free) methods.

Force-fitting experimental data to different model function $f(\alpha)$ is denoted as model-fitting methods, after the $f(\alpha)$ model has been selected from the best linear fit for a series of temperature, $k(T)$ is evaluated (Rodante, *et al.* 2002).

Model-free isoconversional methods allow for estimating the activation energy as function of α without choosing the reaction model, the basic assumption of these methods is that the reaction rate of constant extent of conversion α depends only on the temperature. Hence, constant E_a value can be

expected in the case of single stage decomposition, while for multi-step process E_a varies with α due to the variation in the relative contributions of single steps to the overall reaction rate (Khawam, *et al.* 2005 and Vyazovkin, *et al.* 2002).

Model-fitting Approach

There are several nonisothermal model fitting methods. One of the most popular is the Coats and Redfern method (CR method), which utilizes the asymptotic series expansion in approximating P(x) Eq. (7), producing the following equation

$$\ln \frac{g(\alpha)}{T^2} = \ln \left(\frac{AR}{\beta E_a} \left[1 - \left(\frac{2RT^*}{\beta E_a} \right) \right] \right) - \frac{E_a}{RT} \quad (8)$$

Where T^* is the mean experimental temperature.

The other method proposed by Clark and Kennedy (CK method) is based on the expression, $T = \beta t + T_0$, where T_0 is initial temperature.

The basic equation is:

$$\frac{\beta g(\alpha)}{T - T_0} = A \exp \left(- \frac{E_a}{RT} \right) \quad (9)$$

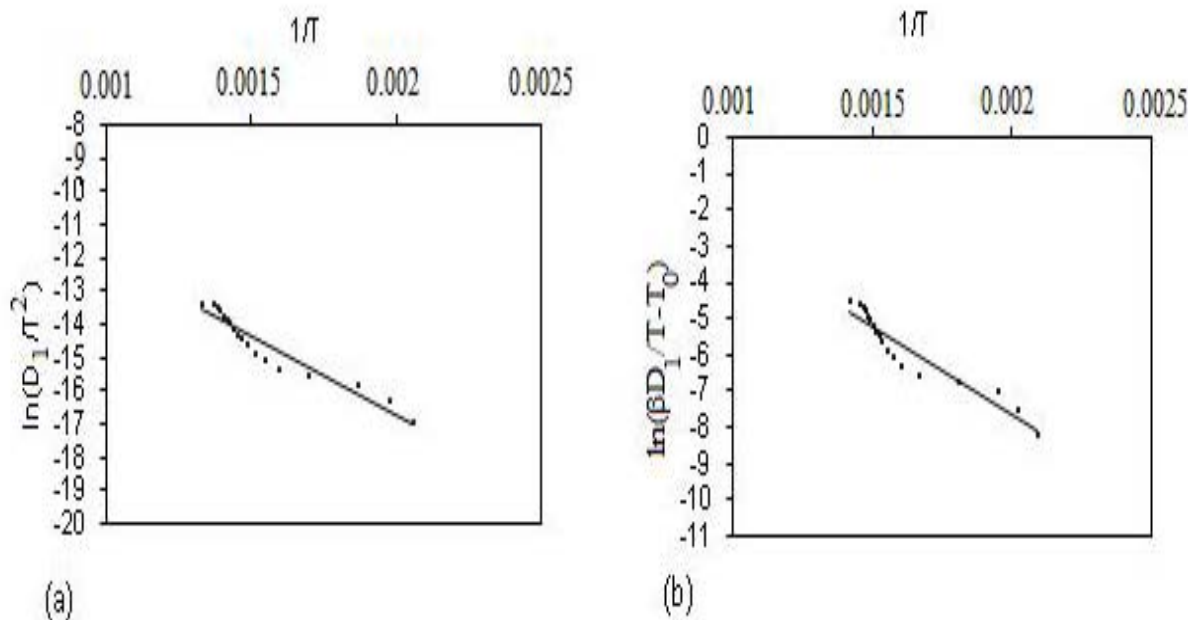


Fig. (5a). CR method and (b)CK method.

Taking the logarithm of both sides of the equation:

$$\ln \frac{\beta g(\alpha)}{T - T_0} = \ln A - \frac{E_a}{RT} \quad (10)$$

Plotting the left-hand side of both equations (8 and 10) against $1/T$ should give straight lines for the reaction models listed in Table 1. (Vyrovkin, *et al.* 1999) and the result are shown in Fig. 5. From the slope and intercept we can determine E_a and $\ln A$ respectively.

The values of activation energy (E_a), pre-exponential factors ($\ln A$) and the coefficients of linear correlations (r) for kinetic models are presented in Table 2. The correlation coefficient (r) is sometimes used as a parameter for choosing the best model.

As listed in Table 2. for both applied methods (CR and CK methods), it can be found that D_1 is the best model show the linear relationships of the data for both irradiated and un-irradiated mixtures. The values of E_a , $\ln A$ (Arrhenius parameters) and r obtained from CR and CK methods using the selected model for the processes obtained in Table 2 are very low. From this fact it may be concluded that the reaction under consideration is a typical complex multi-step reaction with more than one mechanism.

Table 2. Kinetic parameter determined by CR and CK methods

model	C.R						C.K					
	E		lnA		r		E		lnA		r	
	un-irradiated	Irradiated	un-irradiated	Irradiated	un-irradiated	Irradiated	un-irradiated	Irradiated	un-irradiated	Irradiated	un-irradiated	Irradiated
D1	39.2464	40.03058	4.22043	4.314446	91.528	92.324	39.05335	39.99566	2.50784	2.61826	91	91.982
D2	44.26224	45.23348	4.800317	4.925812	89.362	90.384	44.06919	45.13837	3.00946	3.13678	88.806	89.9
D3	50.69728	51.84427	4.901847	5.052753	86.026	87.194	50.50439	51.749	3.01522	3.16666	85.46	86.696
D4	46.70489	47.40077	3.828872	3.957691	88.27	89.344	46.17945	47.30533	2.001	2.13616	87.704	88.85
R3	18.84302	20.95361	0.471686	0.481407	82.33	82.284	18.65013	20.8585	-1.03556	-0.99312	80.712	80.93
R2	20.4275	19.29513	0.419865	0.522472	80.626	83.788	20.23461	19.23261	-1.06906	-0.96554	79.074	82.552
A2	7.04249	-	-	-	55.174	58.306	6.849522	7.212328	-2.1533	-2.10832	50.74	54.498
A3	1.414162	-	-	-	10.664	13.266	1.221194	1.464228	-3.15334	-3.12316	6.954	10.17
A 3/2	12.67087	-	1.043867	-	68.484	70.568	7.482101	12.96053	-1.1533	-1.09346	65.778	68.458
A4	-	-	-	-	18.854	17.928	-	-	-3.72528	-3.63062	18.498	15.686
F1	23.92719	24.55174	2.342056	2.438306	76.942	78.648	23.73431	24.45679	0.84674	0.9363	75.544	77.418
F2	37.05384	38.06748	4.591417	5.691372	66.106	67.818	36.86095	37.97237	3.87932	4.02374	65.174	67.002
F3	53.49527	54.83765	7.313669	9.754276	58.818	60.462	53.13594	54.74254	7.6117	7.8265	58.198	59.924
F3/2	30.01919	30.82133	7.016659	3.937283	71.25	72.98	29.82598	30.72638	2.2576	2.37312	70.098	71.964
P1	-	-	-	-	89.794	90.326	-	-	-4.19572	-4.18152	86.678	86.986
P2	-	-	-	-	47.984	48.426	-	-	-3.8765	-3.86118	45.342	43.424
P3	2.620722	-	-	-	45.912	48.986	2.236749	2.474895	-3.23806	-3.21012	34.73	41.668
P4	26.97411	27.58386	2.119116	2.195114	90.048	91.302	26.78106	27.48874	0.59254	0.67548	89.428	90.606

Model-free approach

The Kissinger–Akahira–Sunose method (KAS method) is based on the Coats–Redfern approximation of $P(x) \approx (\exp(-x))/x^2$ which transformed Eq. (7) to:

$$\ln\left(\frac{\beta}{T}\right) = \ln \frac{AR}{Ea g(\alpha)} - \frac{Ea}{RT} \quad (11)$$

Another method proposed by Tang (T method) is based on the approximate formula which introduced into Eq. (7). Taking the logarithms of both sides, Eq. (12) is obtained as:

$$\ln\left(\frac{\beta}{T^{1.894661}}\right) = \ln\left[\frac{AEa}{Rg(\alpha)}\right] + 3.635041 - 1.894661 \ln Ea - 1.001450 \frac{Ea}{RT} \quad (12)$$

A plot of the left-hand sides of both Eqs. (11 and 12) versus $1/T$ give a group of straight lines at each α (Vyrovkin, *et al.* 1999) as can be seen in Fig. 6, which give apparent activation energy from the slope for a particular α without considering a selected model.

The Vyazovkin isoconversional method (VYZ method) (Vyazovkin, *et al.* 1999 and Janković, *et al.* 2007) is a nonisothermal method which utilizes an accurate nonlinear Senium-Yang approximation of P(x) (Eq. (7)), which leads to:

$$\Omega = \left| \frac{\sum_{i=1}^n \sum_{j \neq i}^n \frac{I(E_{a,\alpha}, T_{\alpha,i}) \beta_j}{I(E_{a,\alpha}, T_{\alpha,j}) \beta_i} \right| \quad (13)$$

$$I(E_{a,\alpha}, T_{\alpha}) = \int_0^{T_{\alpha}} \exp\left(\frac{-E_{a,\alpha}}{RT}\right) dT \quad (14)$$

Where n the number of heating rates, I(E_{a,α}, T_α) the exponential integral (P(x)) that results from heating rate β. The 5th degree Senum-Yang approximation was chosen for our work.

The E_{a,α} can be determined at any particular value of α by finding the value of E_α for which the objective function Ω is minimized.

The temperature integral can be evaluated by several approximation. We have used Gorbachev, Agrawal and Sivasubramanian and Cai for integration of Eq. (14) (Ghoshal, *et al.* 2006 and Maiti, *et al.* 2006).

$$\int_0^T \exp\left(\frac{-E_{\alpha}}{RT_{\alpha i}}\right) dT = \frac{RT_{\alpha i}^2}{E_{\alpha}} \left(\frac{1}{1 + \frac{2RT}{E_{\alpha}}}\right) \exp\left(\frac{-E_{\alpha}}{RT}\right) \quad (15)$$

$$\int_0^T \exp\left(\frac{-E_{\alpha}}{RT_{\alpha i}}\right) dT = \frac{RT_{\alpha i}^2}{E_{\alpha}} \left[\frac{1 - 2RT/E_{\alpha}}{1 - 5(ER/E_{\alpha})^2} \right] \times \exp\left(\frac{-E_{\alpha}}{RT_{\alpha i}}\right) \quad (16)$$

$$\int_0^T \exp\left(\frac{-E_{\alpha}}{RT_{\alpha i}}\right) dT = \frac{RT_{\alpha i}^2}{E_{\alpha}} \left[\frac{E_{\alpha}/RT_{\alpha i} + 0.66691}{E_{\alpha}/RT_{\alpha i} + 2.64943} \right] \times \exp\left(\frac{-E_{\alpha}}{RT_{\alpha i}}\right) \quad (17)$$

Figure 7 shows the variation of apparent activation energy E_{a,α}, as a function of the extent of conversion α of the data for un-irradiated and γ-irradiated mixtures. From Fig. 7 we can recognized that the dependence of Ea,α on α is almost the same by using different isoconversional methods. And

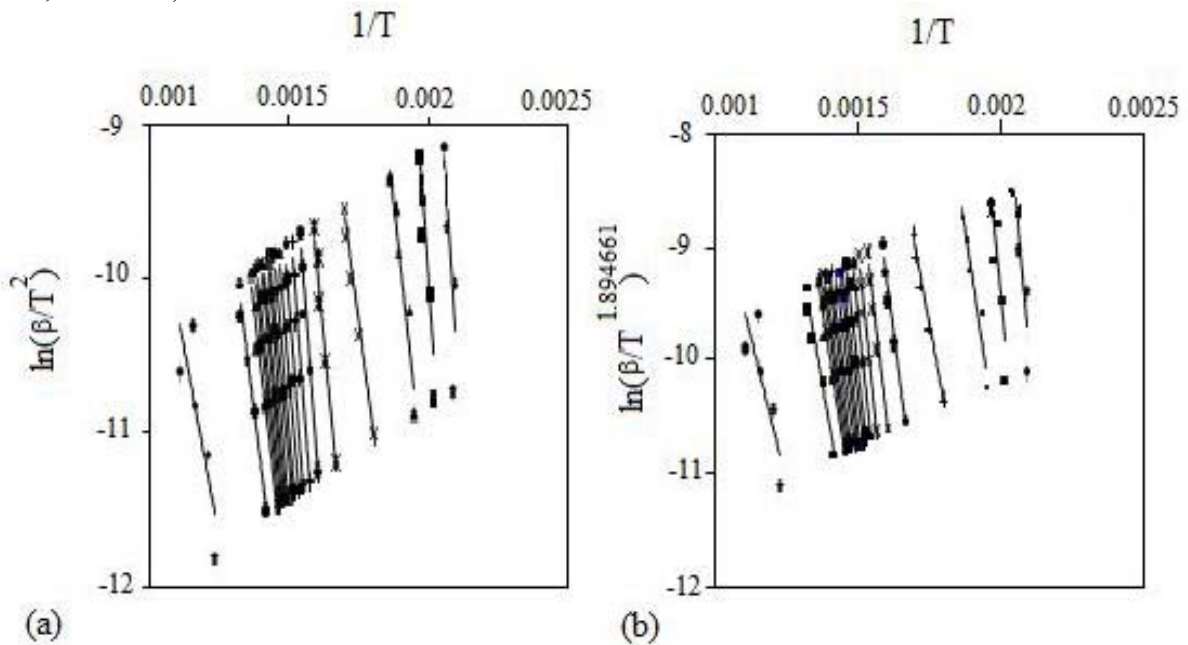


Fig . 6. (a)KAS method, (b)T method.

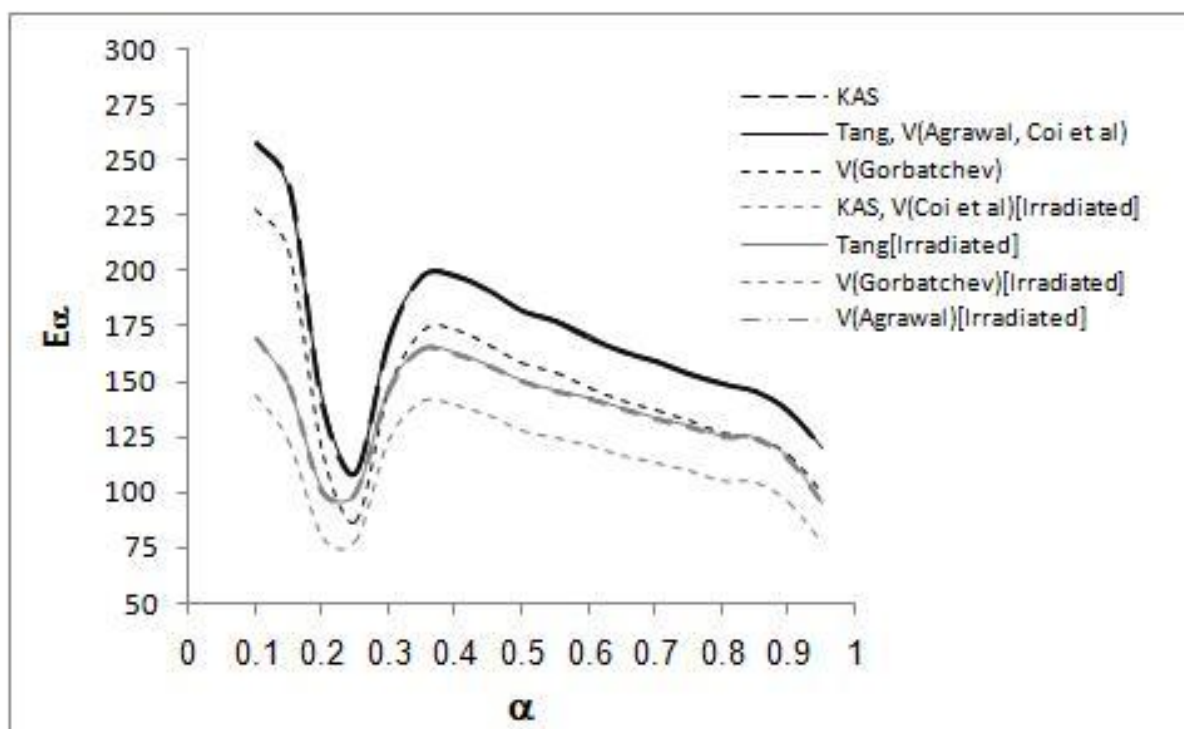


Fig. 7. The activation energy plotted as a function of the extent of the conversion.

these differences in the values of $E_{a,\alpha}$ could be due to the approximation of temperature integral that were used in the derivations of relations that ground KAS, T and VYZ methods (Vyzovkin, *et al.* 1999). Also, fig. 7 shows that, the values of $E_{a,\alpha}$ for γ -irradiated mixture are reduced compared to un-irradiated one. The reducing of the values of activation energy of the decomposition reaction could be attributed to the formation of additional nucleation sites and reactive centers. From the dependence of $E_{a,\alpha}$ on α we can assumed that there are at least two steps, the first step at $\alpha < 0.3$ show decrease of activation energy by increase extant of conversion which is lie to dehydration process, the second step at $\alpha > 0.3$ which is show an increase of the activation energy by increase extent of conversion which lie to decarbonation and formation of the magnesium chromite.

Compensation effect

Use of the artificial isokinetic relationship (IKR) that occurs on fitting various reaction models to the same set of nonisothermal kinetic data can be used to evaluate $\ln A$.

$$\ln A_j = a + bE_{a,j} \quad (18)$$

Where j refers to one of the possible models $f_j(\alpha)$ assumed to describe the process. The parameters of Eq. (18) are $a = \ln k_{iso}$ and $b = 1/RT_{iso}$ (Agrwal, 1986). Figure 8 shows the artificial isokinetic relationship for the process obtained by CK method. The values of a , b , k_{iso} , T_{iso} of Eq. (18) obtained by (CK) model fitting are given in Table 3.

It can be seen that the isokinetic temperatures

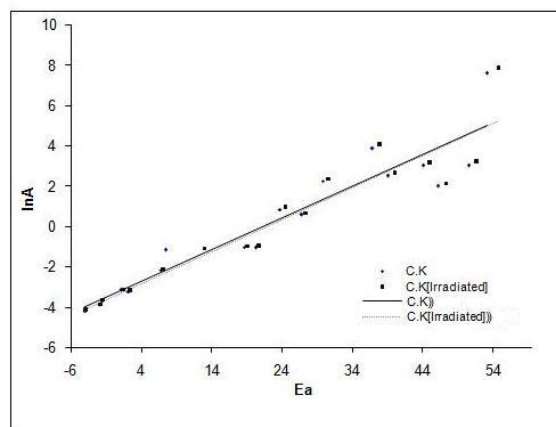


Fig. 8. The isokinetic relationships obtain by CK method.

(T_{iso}) lying in the region of the experimental temperature and this indicates that the reaction model $f(\alpha)$ was properly chosen.

Table.3. Artificial isokinetic parameter obtained by CK method

Method	a (min ⁻¹)	b (mol kJ ⁻¹)	k _{iso} (min ⁻¹)	T _{iso} (K)	r
KC	-3.396	0.158	0.0335	759.82	0.896
KC (irradiation)	-3.488	0.159	0.0306	753.63	0.905

Once the correlation parameters a and b have been evaluated, the $E_{a,\alpha}$ values are substituted for $E_{a,j}$ in Eq. (18) to estimate the corresponding $\ln A_\alpha$ values and obtaining the dependence of $\ln A_\alpha$ on α for multi-step processes (Vyazovkin, *et al.* 1999).

Figure 9 shows the variation of the $\ln A_\alpha$ as a function of extent of conversion α , which was obtained by different isoconversional methods for the process.

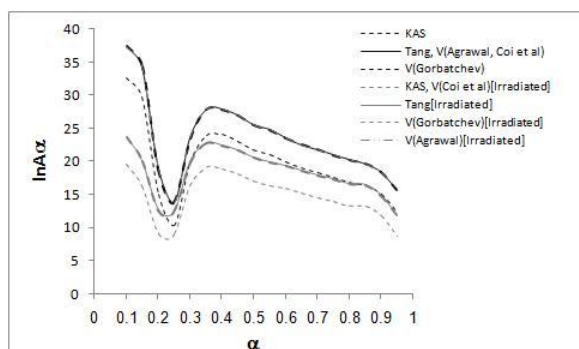
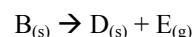
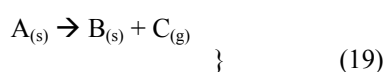


Fig. 9. Dependence of the $\ln A_\alpha$ on extent of conversion, estimated from Eq. (18) for the different isoconversional methods.

It can be seen that the $\ln A_\alpha$ shows the same dependence on α as the apparent activation energy $E_{a,\alpha}$ in Fig. 7. This behavior supported the conclusion mentioned above.

Simulation

Simulated data are the only data for which Arrhenius parameters and reaction models are known exactly (Vyazovkin, 2000). The data were simulated according to the scheme of two reaction mechanisms



The overall reaction rate of these processes is:

$$\frac{d\alpha}{dt} = \frac{1}{2} \left(\frac{d\alpha}{dt} + \frac{d\alpha}{dt} \right)$$

$$= \frac{1}{2} [k_1(T)f(\alpha_1) + k_2(T)f(\alpha_2)] \quad (20)$$

The Arrhenius parameters of the individual steps were taken so that $A_1 = 10^{31} \text{ min}^{-1}$, $E_1 = 260 \text{ kJmol}^{-1}$; $A_2 = 10^{10} \text{ min}^{-1}$ and $E_2 = 80 \text{ kJmol}^{-1}$. The values were chosen to make rates of two steps are comparable within the working range temperature.

Integration of Eq. (20) for nonisothermal condition has give rise to reaction dependence of α vs. T.

By assumption that, the processes contain at least two steps with different reaction mechanism. The first mechanism is third order reaction (F_3) model, and the second mechanism is diffusion in one dimensional (D_1) model. Then the effective activation energy of the overall process can be written as:

$$E_{a,\alpha} = -R \left[\frac{d \ln(d\alpha / dt)}{dT} \right]_\alpha$$

$$= \frac{E_1 k_1(T)f(\alpha_1) + E_2 k_2(T)f(\alpha_2)}{k_1(T)f(\alpha_1) + k_2(T)f(\alpha_2)}$$

$$= \frac{E_1 k_1(T)f(1-\alpha_1)^3 + E_2 k_2(T)f(\frac{1}{2}\alpha_2)}{k_1(T)f(1-\alpha_1)^3 + k_2(T)f(\frac{1}{2}\alpha_2)} \quad (21)$$

This is clearly a function of both temperature an extent of conversion. Substitution of depends of a α verses T for various β into Eq.(21) allows surface plots of the effective activation energy as function of α and β to be obtained (Sbirrazzuoli, *et al.* 2000). These plots are shown in Fig. 10.

Acknowledgements. This work was supported by the King Abdullaziz City of Science and Technology in Saudi Arabia. Also the authors thanks Dr. Ahmed Basfar for his supported and advice

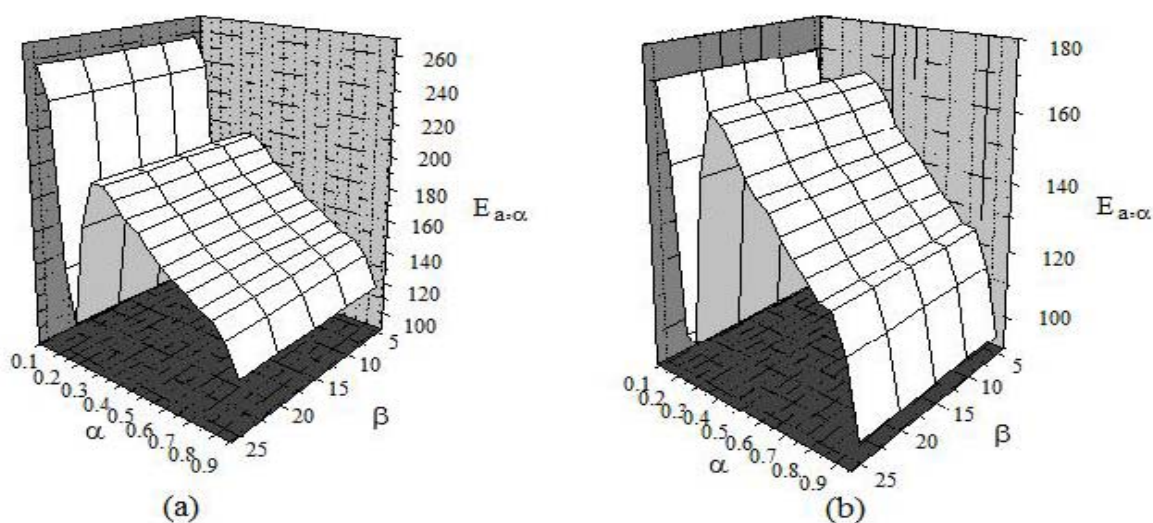


Fig. 10. Surface plot of activation energy for simulated process before irradiation (a) and after irradiation.

References

- Agrwal, R. K., "On the compensation effect", *Journal of Thermal Analysis*, Vol. 31, (1986), 73-86.
- Al-Farhan, K. A., "a qualitative and quantitative PC program for X-ray powder diffraction", *Powder Diffraction*, Vol. 14, No. (1), (1999), 16-21.
- Bhatta, D. and Nayak, H., "Catalytic effects of magnesium chromite spinel on the decomposition of lanthanum oxalate" *Thermochimica Acta*, Vol. 389, (2002), 109-119.
- Criado, J., Gonzalez, F. and Morales, J., "Alteration of kinetics and thermodynamics of thermal decomposition of Alkaline-Earth Carbonates induced by grinding", *Thermochimica Acta*, Vol. 32, (1979), 99-110.
- Docherty, F. T., Craven, A. J., McComb, D. W. and Skakle, J., "ELNES investigations of the oxygen K-edge in spinels" *Ultramicroscopy*, Vol. 86, (2001), 273-288.
- Galway, A. K. and Brown, M. E., *Thermal Decomposition of Ionic Solids*, Elsevier Science B.V., 1999.
- Gengembre, L., Sloczynski, J., Ziolkowski, J., Grzybowska, B., Grabowski, R., Jachewicz, D. and Weislo, K., "Oxidative dehydrogenation of propane on $Ni_xMg_{1-x}Al_2O_4$ and $NiCr_2O_4$ spinels" *Journal of Catalysis*, Vol. 187, (1999), 410-418.
- Ghoshal, A. K. and Saha, B., "Model-free kinetics analysis of waste PE sample", *Thermochimica Acta*, Vol. 451, (2006), 27-33.
- Hartman, M., Trnka, O. and Svoboda, K., "Decomposition Kinetics of Alkaline-Earth Hydroxides and Surface-Area of Their Calcines" *Chemical Engineering Science*, Vol. 49, (1994), 1209-1216.
- Janković, B., Adnadević, B. and Jovanović, J., "Application of model-fitting and model-free kinetics to the study of non-isothermal dehydration of equilibrium swollen poly (acrylic acid) hydrogel: Thermogravimetric analysis", *Thermochimica Acta*, Vol. 452, No. (2), (2007), 106-115.
- Khan, N., Dollimore, D., Alexander, K., Wilburn, F., "The origin of the exothermic peak in the thermal decomposition of basic magnesium carbonate", *Thermochimica Acta*, Vol. 367, (2001), 321-333.
- Khawam, A. and Flanagan, D. R., "Role of isoconversional methods in varying activation energies of solid-state kinetics II. Nonisothermal kinetic studies", *Thermochimica Acta*, Vol. 436, (2005), 101-112.
- Mahfouz, R. M., Monshi, M. A. S., Alshehri, S. M. and Abd El-Salam, N.M., "Isothermal decomposition of γ -irradiated samarium acetate", *Radiation Physics and Chemistry*, Vol. 59, (2000), 381-385.
- Mahfouz, R. M., Monshi, M. A. S., Alshehri, S. M. and Abd El-Salam, N. M., "Kinetics of the thermal decomposition of γ -irradiated cobaltous acetate", *Thermochimica Acta*, Vol. 363, (2000), 61-70.
- Maiti, A. K., Ghoshal, A. K. and Saha, B., "Model-free method for isothermal and non-isothermal decomposition kinetics analysis of PET sample", *Thermochimica Acta*, Vol. 444, (2006), 46-52.
- Monshi, M. A. S., Abd El-Salam, N. M. and Mahfouz, R.M., "Isothermal decomposition of γ -irradiated uranyl acetate", *Thermochimica Acta*, Vol. 322, (1998), 33-37.
- Rodante, F., Vecchio, S. and Tomassetti, M., "Kinetic analysis of thermal decomposition for penicillin sodium salts - Model-fitting and model-free methods", *Journal of Pharmaceutical and Biomedical Analysis*, Vol. 29, (2002), 1031-1043.
- Roy, R., White, W. B. and Muller, O., "Infrared spectra of the chromates of magnesium, nickel and cadmium", *Spectrochimica Acta*, Vol. 25, (1969), 1491-1499.
- Sawada, Y., Yamaguchi, J., Sakurai, O., Uematsu, K., Mizutani, N. and Kato, M., "Thermal decomposition of basic Magnesium Carbonates under high-pressure gas atmospheres", *Thermochimica Acta*, Vol. 32, (1979), 277-291.
- Sawada, Y., Yamaguchi, J., Sakurai, O., Uematsu, K., Mizutani, N. and Kato, M., "Thermogravimetric study on the decomposition of hydromagnesite $4Mg(CO_3) \cdot Mg(OH)_2 \cdot 4H_2O$ ", *Thermochimica Acta*, Vol. 33, (1979), 127-140.
- Sawada, Y., Yamaguchi, J., Sakurai, O., Uematsu, K., Mizutani, N. and Kato, M., "Isothermal differential calorimetry on an exothermic phenomenon during thermal decomposition of Hydromagnesite $4Mg(CO_3) \cdot Mg(OH)_2 \cdot 4H_2O$ ", *Thermochimica Acta*, Vol. 34,

- (1979), 233-237.
- Sbirrazzuoli, N., Vyazovkin, S. and Vincent, L.**, "Comparison of several computational procedures for evaluating the kinetics of thermally stimulated condensed phase reactions", *Chemometrics and Intelligent Laboratory Systems*, Vol. 54, (2000), 53-60.
- Sharp, J., Brindley, G. and Achar, B.**, "Numerical Data for Some Commonly Used Solid State Reaction Equations", *J. American Ceramic Soc.*, Vol. 49, No. (7), (1966), 379-382.
- Shimizu, Y., Kusano, S., Kuwayama, H., Tanaka, K. and Egashira, M., J.** "Oxygen-sensing properties of spinel-type oxides for stoichiometric air/fuel combustion control" *Am. Ceram. Soc.*, Vol. 73, (1990), 818-824.
- Spinks, J. W. T. and Woods, R. J.**, *An Introduction to Radiation Chemistry*. Wiley, New York. (1990).
- Vyzovkin, S. and Wight, C.**, "Model-free and model-fitting approaches to kinetic analysis of isothermal and nonisothermal data", *Thermochimica Acta*, Vol. 340-341, (1999), 53-68.
- Vyazovkin, S.**, "Computational aspects of kinetic analysis. Part C. The ICTAC Kinetics Project — the light at the end of the tunnel?", *Thermochimica Acta*, Vol. 355, (2000), 155-163.
- Vyazovkin, S. and Sbirrazzuoli, N.**, "Learning about epoxy cure mechanisms from isoconversional analysis of DSC data", *Thermochimica Acta*, Vol. 388, (2002), 289-298.
- White, W.**, "Infrared characterization. of water and hydroxyl ion. in the basic magnesium carbonate minerals", *The American Mineralogist*, Vol. 56, (1971), 46-53.
- Williey, R. J., Noirclerc, P. and Busca, G.**, "Preparation and characterization of Magnesium Chromaite and Magnesium Ferrite aerogels", *Chem. Eng. Comm.*, Vol. 123, (1993), 1-16.

التحليل الحراري للانحلال عند تغير درجات الحرارة للخليط البلوري
 $(Mg_5(CO_3)_4(OH)_2 \cdot 4H_2O / 5Cr_2O_3)$

أسماء بنت عبدالله العثمان، خالد بن عبدالرحمن الفرحان، رفعت محمد محفوظ

قسم الكيمياء، كلية العلوم، جامعة الملك سعود، الرياض

المملكة العربية السعودية

البريد الإلكتروني: asmaalothman@yahoo.com

هاتف ٠٠٩٦٦٥٠٧٢٩٢٥٢٧، فاكس ٠٠٩٦٦١٤٨٧٤٥٩٥

(قدم للنشر في ٢٥/١/١٤٢٩هـ؛ وقبل للنشر في ١٣/٤/١٤٢٩هـ)

الكلمات المفتاحية: التحلل الحراري، النموذج المقيد، النموذج الحر، ثبوت الحركة، الدوال الحركية، سبينل $MgCr_2O_4$.

ملخص البحث. تم تحضير سبينل نقي من رفع درجة حرارة الخليط البلوري $(Mg_5(CO_3)_4(OH)_2 \cdot 4H_2O / 5Cr_2O_3)$ عند $900^\circ C$ لمدة ٢٧ ساعة. استخدمت تقنيات TG و DTA و FTIR و XRPD لتتبع التفاعل والتعرف على النواتج. تم دراسة حركية الانحلال الحراري عند تغير درجات الحرارة للخليط البلوري الفيزيائي غير المشع والمشع في الهواء الثابتاً وتقدير الدوال الحركية من خلال تقريبات النماذج المقيدة والحررة وعلاقة ثبوت الحركة للعمليات عديدة الخطوات (IKR). أظهرت النتائج أن انحلال الخليطين (غير المشع والمشع) يتم بخطوتين متتابعين بميكانيكيتين مختلفتين الأولى ميكانيكية التفاعل من الرتبة الثالثة (F) والثانية ميكانيكية الانتشار في بعد واحد (D₁).